Environmental Science
Water Research & Technology

ROYAL SOCIETY OF CHEMISTRY

PAPER

View Article Online
View Journal | View Issue

Cite this: *Environ. Sci.: Water Res. Technol.*, 2025, **11**, 2529

Iodinated disinfection byproduct formation from iohexol in sunlit and chlorinated urban wastewaters

Reagan Patton Witt [a] and Marcelo I. Guzman *[ab]

Iodinated disinfection by-products (I-DBPs) are of growing concern due to their elevated toxicity compared to their chlorinated counterparts, with links to adverse health effects such as bladder cancer and miscarriages. Medical imaging agents like iohexol, commonly used in healthcare facilities, introduce iodine into wastewater systems. This study investigates the photodegradation of iohexol and the subsequent formation of products, including I-DBPs, during simulated final wastewater treatment under chlorination and sunlight exposure. Experiments were conducted with solutions containing 30 μM iohexol, 3 mg L^{-1} humic acids, and 5.5 mg L^{-1} hypochlorite. Samples were irradiated at $\lambda \geq 295$ nm and subject to ion chromatography monitoring of I^-, IO_3^-, Cl^-, and ClO_3^-, providing mechanistic insight into the fate of iodide released from iohexol. UV-visible spectroscopy was employed to monitor the degradation profile of iohexol and the concurrent release of iodide. Electrospray ionization mass spectrometry (ESI-MS) identified a range of anionic products based on their mass-to-charge ratios (*m*/*z*), including low molecular weight carboxylic acids, their carcinogenic haloacetic derivatives (chloroacetic acid (*m*/*z* 93), iodoacetic acid (IAA, *m*/*z* 185), and hydroxyiodoacetic acid (*m*/*z* 201)) as well as phenolic halides. Notably, IAA was present at a concentration of 0.16 μM at the conclusion of the reaction. These findings elucidate photodeiodination-coupled radical attack, photooxidative cleavage, and halogenation transformation pathways of iodinated compounds during disinfection and underscore the potential risks associated with their presence in wastewater. The results provide valuable insights for medical facilities and wastewater treatment plants aiming to mitigate the formation of hazardous I-DBPs.

Received 28th July 2025,
Accepted 11th September 2025

DOI: 10.1039/d5ew00709g

rsc.li/es-water

Water impact

Iodinated disinfection by-products (I-DBPs) are emerging contaminants of significant concern due to their markedly higher toxicity compared to their chlorinated analogs. Studies have shown that I-DBPs exhibit up to 700 times greater cytotoxicity and genotoxicity than regulated chlorinated DBPs. The widespread use of iodinated contrast media (ICM) in hospital radiology departments introduces a substantial source of iodide into wastewater. Upon chlorination and exposure to sunlight, ICM can degrade, releasing iodide that subsequently contributes to form I-DBPs, including carcinogenic haloacetic acids such as iodoacetic acid. Our research provides a mechanistic understanding of these transformation pathways, offering critical insights for improving wastewater treatment strategies and mitigating the formation of toxic I-DBPs in effluents from healthcare facilities.

Introduction

The disinfection of water is one of the most significant public health achievements of the past century. However, the widespread use of chlorine in drinking and wastewater treatment has led to the formation of disinfection byproducts (DBPs), many of which are associated with carcinogenic, mutagenic, and reproductive health risks.[1–7] Over 700 DBPs can form through reactions between disinfectants and natural organic matter (NOM), halides, or anthropogenic pollutants.[8] While regulated DBPs such as trihalomethanes (THMs) and haloacetic acids (HAAs) are routinely monitored by the U.S. Environmental Protection Agency (EPA) in drinking water, many others remain unregulated and undetected.[9,10] Among these emerging contaminants are iodinated disinfection byproducts (I-DBPs), which form during chemical disinfection of water containing iodide or iodinated organic compounds. These include iodo-acids, iodinated trihalomethanes (I-THMs), iodo-amides, and iodo-aldehydes, compounds that exhibit significantly higher genotoxicity and cytotoxicity than their chlorinated and brominated analogs.[9,10]

I-DBPs are typically detected in drinking water at concentrations ranging from nanograms to micrograms per

[a] *Department of Chemistry, University of Kentucky, Lexington, Kentucky 40506, USA. E-mail: marcelo.guzman@uky.edu*
[b] *Lewis Honors College, University of Kentucky, Lexington, Kentucky 40506, USA*

liter, depending on source water composition and disinfection conditions.[10] Their formation is influenced by NOM, iodide levels, disinfectant type (*e.g.*, chlorine, chloramine), and pH.[9] Despite their toxicity, most I-DBPs remain unregulated, and their health impacts (including bladder cancer, reproductive toxicity, and developmental effects) are still under investigation.[10] A major anthropogenic source of iodine in water systems is iodinated contrast media (ICM),[10] such as iohexol,[11] iopamidol, and iomeprol, which are widely used in medical imaging. These compounds are excreted largely unmetabolized and enter wastewater systems, where conventional treatment fails to effectively remove them.[11] As a result, ICMs have been detected in surface water, groundwater, and even finished drinking water globally.[11] Their persistence and transformation during disinfection, particularly under chlorination and chloramination, can lead to the formation of toxic I-DBPs.[9] For instance, chlorination of iopamidol has been shown to produce high levels of I-THMs and iodo-acids.[9]

The formation of I-DBPs in wastewater is not only a concern for drinking water safety (due to potential reuse or infiltration into potable water sources) but also poses ecological risks to aquatic organisms in receiving water bodies. Studies have shown that conventional drinking water treatment methods are often ineffective at removing ICM, leading to the formation of toxic I-DBPs in finished drinking water.[12] Additionally, the persistence and bioaccumulation of DBPs in aquatic environments can disrupt ecosystem stability and harm fish and other aquatic organisms.[13] These dual concerns underscore the importance of understanding I-DBP formation pathways, especially given the increasing discharge of ICMs and the widespread use of chlorination in wastewater treatment.[10]

Although I-DBPs typically occur at lower concentrations (1.7–10.2 μg L^{-1}),[6–8] their toxicity is disproportionately high. For example, iodoacetic acid is 287.5× more toxic than its chlorinated analogue and 3.2× more toxic than its brominated counterpart.[8] While iodide naturally occurs in saline waters and is often considered the primary source of I-DBP formation in coastal regions,[8,14,15] its concentration in many freshwater systems is insufficient to explain observed levels, suggesting additional anthropogenic inputs. One such input is ICM discharge, *e.g.*, iohexol, from healthcare facilities. For example, between 2021 and 2024, the University of Kentucky Health Care System discharged an estimated 9.3–14.2 kg of iohexol per day into Lexington's wastewater infrastructure.[16] These compounds are poorly removed by conventional wastewater treatment, with effluent concentrations reaching up to 15 μg L^{-1}.[12,17–19] With ICM usage increasing by 150% during this period, mitigating their release is critical to reducing I-DBP formation. Most U.S. wastewater treatment plants rely on chlorination for disinfection.[20] Many also use natural sunlight exposure in open basins as a cost-effective method to degrade pollutants prior to final disinfection.[21] However, the combined effects of sunlight and chlorination on I-DBP formation remain poorly understood. This study investigates the transformation of iohexol under simulated wastewater treatment conditions, focusing on sunlight and chlorination pathways. The goal is to elucidate degradation mechanisms and I-DBP formation, providing insight into the environmental fate of ICMs and their contribution to emerging water contaminants.

Experimental

Chemicals

Experiments used an iohexol (Omnipaque) oral solution containing 9.1 mg mL^{-1} iodine, 19.7 mg mL^{-1} iohexol, 1.26 mg mL^{-1} tromethamine, and 0.102 mg mL^{-1} edetate calcium disodium. Solutions of 10.0 to 100 mM hydrochloric acid (EMD Millipore, ACS grade) and 100 mM sodium hydroxide (AMRESCO, ACS grade) were used to adjust the pH of experiments at 7.0. A solution of 37.5 mg L^{-1} humic acids (IHSS Suwanee River II, 52.63% C, ~1061 g mol^{-1})[22] was used as a source of natural organic matter. Calcium hypochlorite (Thermo Scientific, 66.22%) was prepared daily in chlorine free ultrapure water (18.2 MΩ cm^{-1} ELGA Purelab Flex, Veolia) to simulate chlorine treatment. When necessary, sodium thiosulfate (Sigma-Aldrich, 98.84%) was added to quench residual active chlorine and prevent further oxidative reactions. Phenylglyoxilic acid (PGA, Alfa Aesar, 99.9%) was used for actinometry, with benzaldehyde (Sigma-Aldrich, 99.9%) serving as the calibration product. Solutions for liquid chromatography were prepared using a 10.0 mM formate buffer (ammonium formate, Sigma-Aldrich, 99.0%; formic acid, Fisher Optima LC/MS, 99.5%) at pH 3.0, and acetonitrile (J.T. Baker LC/MS, 100.0%) as the organic solvent. Additionally, for direct infusion electrospray ionization (ESI) mass spectrometry (MS) in the negative ionization mode samples were prepared to include 20% v/v methanol (J.T. Baker LC/MS, 100.0%).

Simulated wastewater treatment reactions

The University of Kentucky Hospitals consume 14.2 kg per day of iodinated contrast agent (ICM), which are assumed to be transferred to the main wastewater treatment plant in Lexington (Town Branch Wastewater Treatment Plant). This plant processes ~30 million gallons of water per day.[23] Accordingly, it is estimated that in the wastewater effluent at this facility, $[\text{iohexol}]_{\text{effluent}} \approx 0.15$ μM. To enable the detection and quantification of transformation products under controlled laboratory conditions, [iohexol] was scaled up ~200× relative to the estimated environmental levels. This adjustment was necessary due to the low estimated $[\text{iohexol}]_{\text{effluent}}$, which fall below the sensitivity threshold for product identification and mechanistic analysis. Thus, experiments were performed with a 30 μM solution of iohexol, 3 mg L^{-1} of humic acids, and 5.5 mg L^{-1} of ClO^- at pH 7.00 to simulate relevant conditions at the final wastewater treatment stage.[20,24,25] While this concentration exceeds environmentally relevant levels, it allows for the observation of reaction pathways and product formation that

are expected to occur similarly at lower concentrations, albeit at reduced rates. The insights gained from these experiments are therefore applicable to real-world scenarios and help elucidate the fate of iohexol and its byproducts during wastewater treatment.

At pH 7.00, given the pK_a of HClO is 7.40,[26] the acid (HClO) and its conjugate base (ClO^-) are present at approximately 71.5% and 28.5%, respectively. The [NOM] can vary heavily with location, topography, and seasonal changes with dissolved organic carbon (DOC) values between 2 and 30 mg C L^{-1} for wastewater effluents,[25,27] where humic substances contribute to 40–60% of this DOC.[28] Thus, the amount of chlorine added to wastewater can vary (5–20 mg L^{-1}) to target the characteristics of influent wastewater, affecting the pH of effluent wastewater to fall in the range 6.5–8.5.[20,24]

A calibrated pH meter (Thermo Scientific) was used to pH-adjust all solutions by dropwise addition of sodium hydroxide and hydrochloric acid solutions. Iohexol and humic acids were added into the solution first, followed by the addition of freshly prepared calcium hypochlorite immediately before irradiation. Irradiation of a 3.00 mL solution took place in a 1.00 cm optical path fused silica cuvette with a 1.0 kW Newport Xe–Hg lamp (Scheme 1). Light was filtered through water to remove infrared light followed by a $\lambda_{cut\text{-}off} \geq 295$ nm cut-off filter simulating sunlight conditions.[29–33]

Chemical actinometry was conducted using 5.00 mM phenylglyoxylic acid (PGA) at pH 1.0 to measure photon flux, attenuated to 10.13% of full lamp intensity using neutral density filters, as previously established in our lab.[30,31,34] This concentration of PGA provided a near-UV absorbance profile comparable to that of the experimental system. The decay of PGA was monitored by high pressure liquid chromatography (HPLC, Agilent 1100) using a ZORBAX SB-CN column (3.5 μm, 3.0 × 100 mm) with UV detector set at λ = 260 nm. Undiluted samples were injected (5.0 μL) into the column. The isocratic flow (0.5 mL min^{-1}) consisted of 5% solvent A, a 10.0 mM formate buffer and 95% solvent B, acetonitrile. Elution over 16 min allowed for the separation of PGA and benzaldehyde. The attenuated (10.13% of the total) incident photon flux at $\lambda_{cut\text{-}off} \geq 295$ nm was $I_0 = 1.50 (\pm 0.02) \times 10^{-5}$ einstein per L per s. The absorbed photon flux (I_a) in einstein per L per s was obtained considering the action spectra of the experiment with the lamp in the wavelength interval from 320 to 370 nm based on eqn (1),

$$I_a = I_0\left(1 - e^{-2.303l(\varepsilon_I[\text{iohexol}]_0 + \varepsilon_{HA}[\text{humic acids}]_0)}\right) \quad (1)$$

and used to calculate the quantum yield (ϕ) with eqn (2).

$$\phi = \frac{R_0}{I_a} \quad (2)$$

In the above equations l = 1.00 cm is the reactor path length, ε_I is the molar absorptivity (M^{-1} s^{-1}) of iohexol at a given wavelength (288 M^{-1} s^{-1} at 320 nm, 76.7 M^{-1} s^{-1} at 345 nm, and 83.7 M^{-1} s^{-1} at 370 nm), $[\text{iohexol}]_0$ = 30 μM is the initial concentration of iohexol, ε_{HA} is the molar absorptivity of humic acids at a given wavelength (0.0137 L mg^{-1} s^{-1} at 320 nm, 0.0103 L mg^{-1} s^{-1} at 345 nm, 0.00742 L mg^{-1} s^{-1} at 370 nm), $[\text{humic acids}]_0$ = 3 mg L^{-1} is the initial concentration of humic acids, and R_0 is the initial reaction rate of iohexol loss.

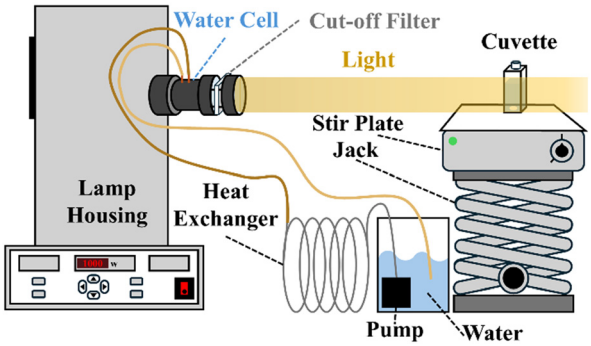

Scheme 1 Photochemical setup with a 1.0 kW Xe (Hg) lamp filtered through water to remove infrared radiation, and equipped with a cut-off filter at $\lambda_{cut\text{-}off} \geq 295$ nm.

Iohexol and product monitoring

Samples underwent analysis by UV-visible spectroscopy (Thermo Scientific, Evolution 220) over 10 min in a 1.00 cm optical path fused silica cuvette. The timescale selected for this study is relevant to the chlorination contact time (~15 min) during urban wastewater tertiary treatment at the Town Branch Water Treatment Plant.[35] The loss of iohexol was monitored at λ = 245 nm and the production of iodide at λ = 223 nm.[36–38] Triplicate experiments were conducted with data representing the mean with error bars corresponding to one standard deviation. Ion chromatography (IC) (Thermo Scientific, Dionex ICS-2000) was used to monitor the formation of iodide and iodate after separation in an IonPack AS11-HC (2 mm × 250 mm) column. To minimize the possible underestimation of halogenated disinfection byproducts during sample handling for IC, as highlighted by Fang *et al.* (2023),[39] a targeted strategy was implemented. All samples for IC were treated with sodium thiosulfate at a controlled molar ratio ($[S_2O_3^{2-}] = 1.4 \times [ClO^-]$) to effectively quench residual chlorine while avoiding excess that could degrade unknown DBPs. Samples were analysed immediately after quenching and stored in the dark under temperature-controlled conditions to suppress chemical degradation. These measures preserved the integrity of halogenated DBPs and enabled a more accurate characterization of their profile during iohexol chlorination under illumination.

For the detection and identification of organic iodinated disinfection byproducts, including iodoacetic acid (IAA), ESI-MS (Thermo Scientific, MSQ Plus) was used in the negative ionization mode to detect anions in experiments and controls. Samples were prepared in 20% v/v methanol and infused at 50 μL min^{-1} with a syringe pump (Harvard Apparatus, Elite Series). Anions were identified based on their mass-to-charge

ratio (m/z) within the range of 30–1000 amu, using a threshold of 1100 ion counts to ensure reliable detection. No thiosulfate was added to these samples. ESI conditions were optimized at 70 psi N_2(g) for nebulizing pressure, −2.5 kV for nebulizing voltage, 40 V for the cone voltage, and a drying gas temperature of 350 °C. A solvent background of 20% methanol in water was subtracted from all spectra. A series 1 pump (Lab Alliance) provided background water flow of 150 μL min^{-1} creating a 4× dilution during the infusion of samples.

Results and discussion

Phototreatment of Iohexol and associated matrix components

Iohexol, hypochlorite, and humic acids were individually and collectively examined under simulated sunlight irradiation to assess their photochemical reactivity and interactions. The growth of new peak at λ = 223 nm corresponds to the production of free iodide (I^-). Under the experimental conditions, it is confirmed that sunlight wavelengths can eject iodine atoms ($I^\bullet$) present in iohexol, to create I^-. The changes in absorbance (ΔA_λ) for iohexol and iodide (I^-) are presented in the insets of Fig. 1, and summarized in Table 1 for a t = 5 min reaction. Fig. 1A shows the UV-visible changes during irradiation of iohexol in the matrix with hypochlorite and humic acids. The decay of iohexol was registered at λ = 245 nm, for a 5 min irradiation example of the complete experimental matrix, the absorbance changes were $\Delta A_{223\ nm} = 2.40 \times 10^{-1}$ and $\Delta A_{245\ nm} = -2.49 \times 10^{-1}$. When iohexol and hypochlorite were irradiated in the absence of humic acids (Fig. 1B), the observed changes were $\Delta A_{223\ nm} = 1.38 \times 10^{-1}$ and $\Delta A_{245\ nm} = -3.22 \times 10^{-1}$. In contrast, irradiation of iohexol with humic acids but without hypochlorite (Fig. 1C) resulted in $\Delta A_{223\ nm} = 2.50 \times 10^{-1}$ and $\Delta A_{245\ nm} = -1.93 \times 10^{-1}$. For the system containing hypochlorite and humic acids without iohexol (Fig. 1D), the absorbance changes were $\Delta A_{223\ nm} = -5.73 \times 10^{-2}$ and $\Delta A_{245\ nm} = -4.41 \times 10^{-2}$. Finally, the dark control containing iohexol, hypochlorite, and humic acids (Fig. 1E) showed negligible changes in $\Delta A_{223\ nm}$ and $\Delta A_{245\ nm}$, confirming the stability of iohexol and the matrix in the absence of light.

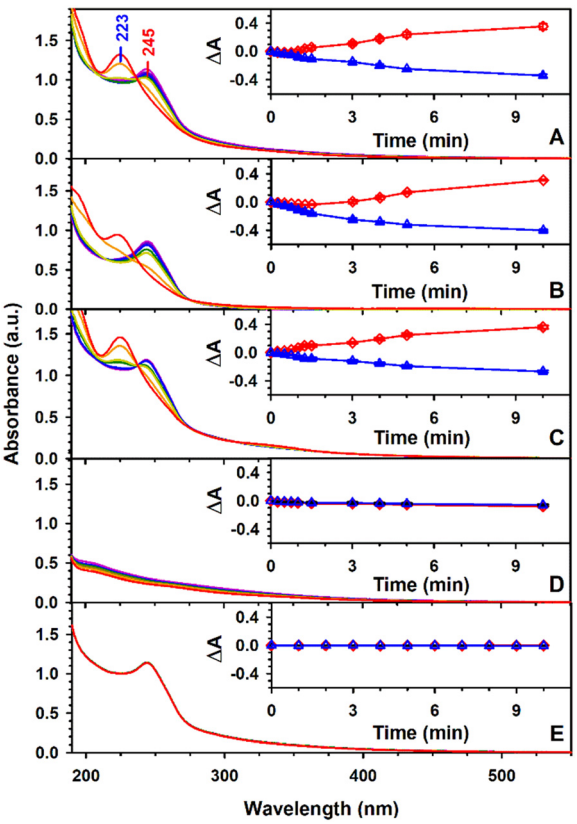

Fig. 1 UV-visible analysis during irradiation ($\lambda_{cut\text{-}off} \geq$ 295 nm) at pH 7.0 of (A) experiment with 30 μM iohexol, 3.0 mg L^{-1} humic acids, and 5.5 mg L^{-1} ClO^-; (B) control A in the absence of humic acids, (C) control B in the absence of ClO^-; (D) control C in the absence of iohexol; and (E) control D in the absence of light. Monitored at irradiation time of (pink) 0, (purple) 0.25, (blue) 0.5, (green) 1, (yellow) 1.5, (orange) 5, and (red) 10 min. Insets display the mean absorbance change with time ($\Delta A_\lambda = A_t - A_0$) for (red diamond) iodide at λ = 223 nm and (blue triangle) iohexol at λ = 245 nm. Error bars are represented but are smaller than the symbols.

The data in Fig. 1 and Table 1 indicate that the increase in absorbance at λ_{max} = 223 nm originated from the release of iodine from the iohexol ring. Mechanistically, deiodination can proceed *via* three primary pathways: (1) direct photolysis through cleavage of the carbon–iodine bond,[40] (2) substitution by hydroxyl radicals,[41] or (3) substitution by chlorine species.[42] Upon irradiation, the carbon–iodine bond can be broken, leading to the formation of an iodine radical, as illustrated in Scheme 2.[40] Deiodination in the 250–400 nm range has been attributed to the singlet ground state to singlet excited state, $S_0 \rightarrow S_1$, electronic transition.[40] When iohexol is excited to its singlet excited state (reaction R1, Scheme 2), an iodine radical is released, forming an iohexol radical intermediate (reaction R2).[43] This singlet radical may undergo electron transfer (reaction R3), resulting in the formation of iodide.[43]

For example, related α-tocopheroxyl radical reacts with O_2(aq) with $k_{R5} \approx 1 \times 10^5$ M^{-1} s^{-1},[44] which is used here to calculate the rate of reaction R5. This yields a value of 26 × [PhO$^\bullet$] s^{-1} for an experimental level of [O_2(aq)] = 2.6×10^{-4} M. The rate constant for reaction R7 should be diffusion-controlled, and is assumed here to be in the order of 10^9–10^{10} M^{-1} s^{-1}. The chlorine atoms participating in reaction R7 arise from photolysis reactions R8 and R9.

$$ClOH \xrightarrow{h\nu} {}^\bullet OH + Cl^\bullet \quad (R8)$$

$$ClO^- \xrightarrow{h\nu} {}^\bullet OH + Cl^\bullet + O_3 \quad (R9)$$

which under present experimental conditions must be [Cl$^\bullet$] < 1×10^{-12} M,[45] based on photolysis rate constants,[46] quantum yields,[47] and availability of the acid and base forms. Therefore, the reaction R7 rate is $\leq 10^{-2} \times$ [PhO$^\bullet$] s^{-1}, which is 2600× slower than reaction R5. Additionally, despite the

Table 1 Experiment and controls for the photooxidation reaction in water with absorbance change ($\Delta A_\lambda = A_t - A_0$) at wavelength ($\lambda$) after t = 5 min irradiation for data in Fig. 1

	Conditions				$\Delta A = A_t - A_0$	
	Iohexol	Humic acids	Light	ClOH	λ = 223 nm	λ = 245 nm
Experiment	Yes	Yes	Yes	Yes	2.40×10^{-1}	-2.49×10^{-1}
Control A	Yes	No	Yes	Yes	1.38×10^{-1}	-3.22×10^{-1}
Control B	Yes	Yes	Yes	No	2.50×10^{-1}	-1.93×10^{-1}
Control C	No	Yes	Yes	Yes	-5.73×10^{-2}	-4.41×10^{-2}
Control D	Yes	Yes	No	Yes	-2.43×10^{-3}	-4.58×10^{-3}
Control E	Yes	No	Yes	No	1.55×10^{-1}	-1.52×10^{-1}
Control F	No	Yes	Yes	No	8.30×10^{-3}	-3.86×10^{-3}

expected [I$^\bullet$] < [Cl$^\bullet$], the electron transfer pathway may still contribute modestly to the formation of hydroxylated products in this system. Thus, the formation of hydroxylated products *via* reactions R5 and R6 appears to be the predominant pathway for the transformation of phenoxyl radicals in Scheme 2.

Iodine atoms photoreleased from the aromatic ring can contribute to the formation of I-DBPs through two primary pathways: (1) the oxidation of I$^-$, released from compounds like iohexol, by ClOH to form HOI *via* reaction R10, followed by its reaction with organic matter (*e.g.*, iohexol, humic acids) represented as $C_xH_yO_z$ to yield I-DBPs (reaction R11); and (2) direct halogenation of organic compounds by chlorinated species, as illustrated in Scheme 2.

$$\mathrm{ClOH + I^- \rightarrow HOI + Cl^-} \quad \text{(R10)}$$

$$\mathrm{C_xH_yO_z + HOI \rightarrow I\text{-}DBPs} \quad \text{(R11)}$$

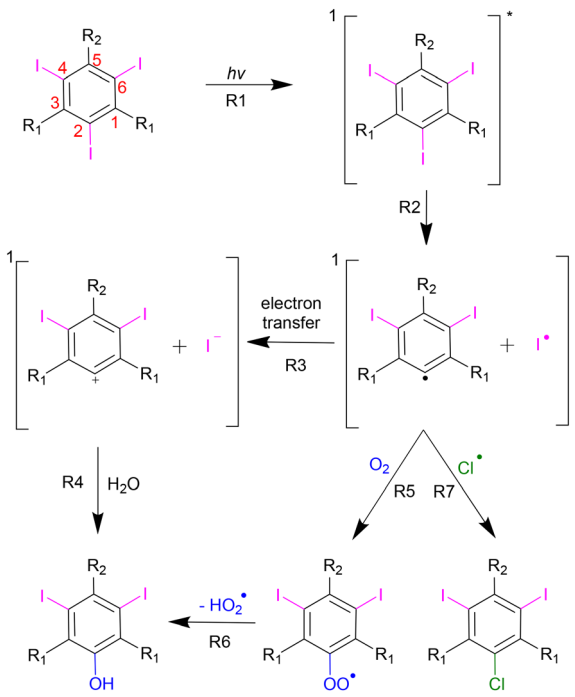

Scheme 2 Proposed deiodination of iohexol *via* direct photolysis.

These pathways highlight the role of reactive iodine species, particularly HOI, in driving I-DBP formation under the studied conditions.

Although high-molecular weight DBPs have been shown to be cytotoxic, their toxicity is relatively low compared to that of low-molecular weight DBPs, such as smaller haloacetic acids like iodoacetic acid (IAA).[48,49] Mechanisms underlying DBP formation, *e.g.*, such as the generation of smaller haloacetic acids and chlorine-substituted iohexol, have been well-documented in various studies.[15,50,51]

As shown in Table 1, in the absence of hypochlorite (Fig. 1C), the degradation of iohexol registered at λ = 245 nm is reduced compared to the full experiment (Fig. 1A) by 5.6×. This decrease is attributed to the diminished presence of hydroxyl radicals, which are proposed to form *via* hypochlorous acid and hypochlorite photolysis, as described in reactions R8 and R9, respectively.[47]

As shown in Table 1, the $\Delta A_{245\ \mathrm{nm}}$ value indicates a 29.9% reduction in iohexol degradation in the presence of humic substances (Fig. 1A) compared to control A without them (Fig. 1B). This notable decrease underscores the inhibitory role of humic acids on photodegradation, likely due to their competition with iohexol for sunlight and reactive species. By absorbing light and scavenging radicals, humic acids diminish the formation of hydroxyl radicals and other intermediates essential for deiodination. This competition slows the degradation kinetics of iohexol, effectively extending its lifetime in solution.

Another source for the generation of HIO is shown in reaction R12 for the oxidation of photo-released I$^-$ by ClO$^-$:

$$\mathrm{I^- + ClO^- + H_2O \rightarrow HIO + Cl^- + HO^-} \quad \text{(R12)}$$

Moreover, the excess hypochlorous acid also available for iohexol to react in the absence of humic acids (Fig. 1B) leads to the formation of iodate *via* reaction R13 with a rate constant k_{R13} = 8.2 M^{-1} s^{-1} at 25 °C.[14]

$$\mathrm{HOI + 2HOCl \rightarrow IO_3^- + 2Cl^- + 3H^+} \quad \text{(R13)}$$

The formation of iodate in reaction R13 is supported by the spectral broadening observed in the 190–200 nm region of Fig. 1B as a partial new peak, suggesting the formation of an intermediate species.[15,38,52] As illustrated in Fig. 1C, the

absence of hypochlorite results in reduced spectral broadening in the 190–200 nm region compared to Fig. 1B. In contrast, both the experiment and control A (Fig. 1A and B) contain hypochlorous acid, which can further react with organic constituents to produce chlorinated disinfection byproducts (Cl-DBPs) *via* reaction R14.

$$C_xH_yO_z + ClOH \rightarrow Cl\text{-}DBPs \quad (R14)$$

The reaction kinetics of iohexol degradation occur rapidly within the first few minutes of the 10 min irradiation period studied above, as shown in Fig. 2. Monitoring these early stages provides more accurate mechanistic insights and avoids potential misinterpretations that may arise when intermediate or secondary products begin to dominate and influence the observed reactivity. Fig. 2 illustrates the high temporally resolved changes in relative iohexol concentration for the experiment and controls in Table 1. In the absence of light, chlorination alone has minimal impact on iohexol degradation, suggesting that hypochlorite would be ineffective at producing I-DBPs without photolytic activation. Upon exposure to light ($\lambda \geq 295$ nm), degradation of iohexol begins, and the presence of hypochlorite further enhances this process. An attempt to explore the advanced oxidation process (AOP) by hydroxyl radical production from *p*-hydroquinone and HClO (see Scheme S1) on iohexol degradation is provided in Fig. S2 (SI).

Notably, the presence of humic acids in the experiment of Fig. 1 significantly suppresses iohexol degradation, likely due to competitive interactions with reactive species. The most effective degradation is observed in control A (without humic acids), which is expected to result in the highest iodine release. Initial degradation rates (R_0), determined from the early linear portion of the kinetics in Fig. 2, were combined with the absorbed photon flux (I_a) to calculate the wavelength-dependent quantum yield (Φ_λ) using eqn (2). These values, summarized in Table 2, facilitate cross-study comparisons of iohexol photoreactivity in complex matrices, enhancing our understanding of sunlight-driven processes in wastewater treatment. Quantum yields are reported at λ = 320, 345, and 370 nm, wavelengths selected to reflect the unique absorbance characteristics of the actinometer, iohexol, and humic acids, respectively, within the near-UV region.

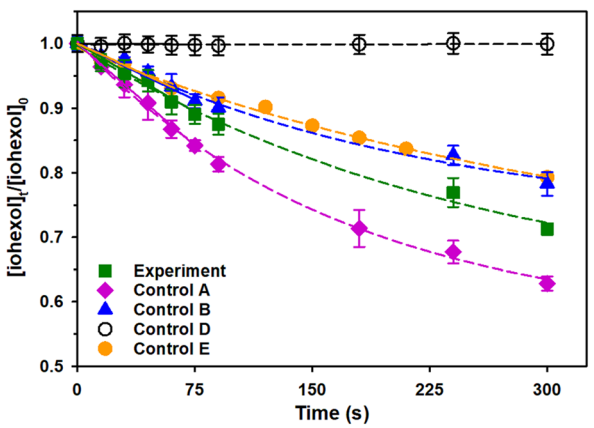

Fig. 2 Decay of iohexol relative to its initial concentration based on UV-visible analysis at λ = 245 nm during irradiation ($\lambda_{cut\text{-}off} \geq 295$ nm) for (green square) experiment with 30 μM iohexol, 3.0 mg L^{-1} humic acids, and 5.5 mg L^{-1} ClO^-; (pink diamond) control A in the absence of humic acids, (blue triangle) control B in the absence of ClO^-; (black open circle) control D in the absence of light; and (orange circle) control E in the absence of both humic acids and ClO^-. Initial reaction rates (R_0) given in Table S1 are represented by solid-colored lines while dashed lines are used as a visual aid only.

IC analysis enabled the monitoring of iodide, iodate, chloride, and chlorate during the irradiation period. As shown in Fig. 3, irradiation of iohexol in the presence of hypochlorite led to a pronounced increase in both iodide and iodate concentrations, following the photolytic cleavage of iodine from the aromatic ring, as previously indicated by UV-visible spectral changes. Humic acids would interfere with this analysis, and therefore Fig. 3 corresponds to control A. Over time, a decline in free iodide is observed, consistent with its oxidation by hypochlorous acid to form HOI *via* reaction R10 as discussed above.[15,52] As previously discussed, HOI is a highly reactive intermediate that cannot be detected by IC, as it rapidly reacts with HClO to form iodate *via* R13. In the presence of organic matter (*e.g.*, humic acids), HOI also contributes to I-DBP formation through reaction R11.[15,52]

Since thiosulfate was added to each aliquot at the time of sampling to quench residual hypochlorite, the presence of thiosulfate and its oxidation product, sulfate, in the chromatograms of Fig. 3 is expected. Iodate is often considered a terminal sink for iodine due to its chemical stability and limited reactivity, *i.e.*, with humic substances.[52] Previous studies have shown that secondary reactions leading to iodate formation occur more rapidly than those forming I-DBPs during chlorination, which helps explain the iodide production observed in control A (Fig. 1B) relative to the experiment (Fig. 1A).[51] During the irradiation of iohexol alone, chloride is detected even in the absence of added hypochlorite. This is attributed to chloride-containing additives in the Omnipaque formulation and pH adjustment reagents. As previously noted, iodate and chlorate are absent under these conditions, confirming that their formation requires the presence of hypochlorite. In contrast, when hypochlorite is irradiated alone, it produces chlorate, consistent with its known degradation pathways. Specifically, chlorate arises from the sequential reactions R15 and R16,

$$2\ ClO^- \rightarrow Cl^- + ClO_2^- \quad (R15)$$

Table 2 Quantum yield (Φ_λ) for the degradation of iohexol at λ = 320, 345, and 370 nm

	$\Phi_{320\ nm}$ (%)	$\Phi_{345\ nm}$ (%)	$\Phi_{370\ nm}$ (%)
Experiment	0.25	0.37	0.50
Control A[a]	2.11	7.87	7.21
Control B[b]	0.21	0.31	0.41

[a] No humic acids. [b] No ClO^-.

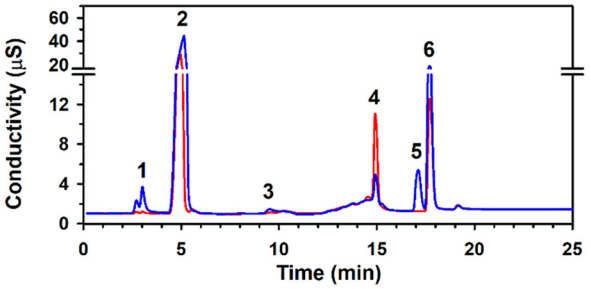

Fig. 3 Ion chromatograms at (red) 0 min and (blue) 7 min of irradiation ($\lambda \geq 295$ nm) for control A at pH 7.0 for 30 μM iohexol with 5.5 mg L^{-1} ClO^-. Retention times (t_r) for identified eluting species (see Table S2) are as follows: (1) iodate, t_r = 2.68 min; (2) chloride, t_r = 4.60 min; (3) chlorate, t_r = 9.93 min; (4) sulfate, t_r = 14.85 min; (5) iodide, t_r = 17.09 min; and (6) thiosulfate, t_r = 17.55 min.

$$ClO_2^- + ClO^- \rightarrow Cl^- + ClO_3^- \quad (R16)$$

which proceed with rate constants $k_{R15} = 2.48 \times 10^{-6}$ M^{-1} s^{-1} and $k_{R16} = 9.7 \times 10^{-4}$ M^{-1} s^{-1}, both reported at 40 °C.[53]

Identification of iodinated products

ESI-MS was used to identify I-DBPs and to elucidate the contributions of individual components in the matrix to the formation of hazardous species. Mass spectra for the experiment and relevant controls are presented in Fig. 4 and 5. Fig. 4 presents solvent background-subtracted mass spectra at 0 and 10 min, while Fig. 5 shows 10 min spectra corrected by subtracting their respective 0 min baselines. Iohexol, with a molecular weight of 821.14, is detected at 0 min in Fig. 4 as a monoanion at *m/z* 820, corresponding to the loss of a proton. A prominent peak at *m/z* 856 is also observed, attributed to a chloride adduct. This assignment is supported by the presence of a +2 Da isotopic peak at *m/z* 858, consistent with the natural abundance of ^{37}Cl. The isotopic distribution ratio at *m/z* 856 : 857 : 858 : 859 observed for the assigned adduct ion, $C_{19}H_{26}O_9N_3I_3Cl^-$, is within experimental error of the theoretical values of 100.0%, 22.0%, 36.3%, and 7.7%, as shown in Fig. S3.

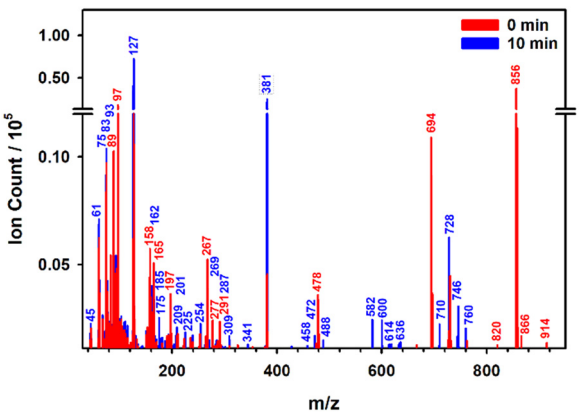

Fig. 4 Electrospray ionization-mass spectrometry (ESI-MS) analysis of experiment with 30 μM iohexol, 3.0 mg L^{-1} humic acids, and 5.5 mg L^{-1} ClO^- at pH 7.0 after (red) 0 and (blue) 10 min irradiation ($\lambda_{cut\text{-}off} \geq 295$ nm). The *m/z* values are labeled in colors corresponding to the spectra with the largest intensity. Each spectrum was corrected by subtracting the corresponding solvent background.

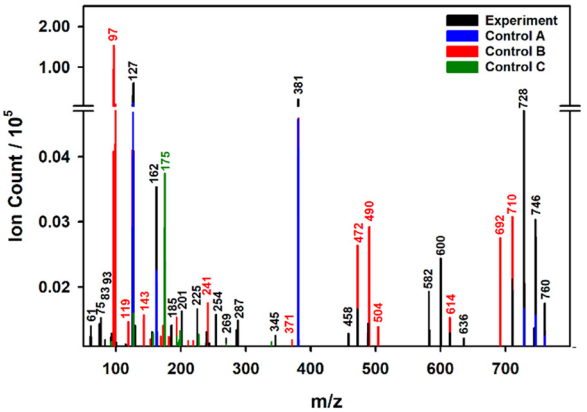

Fig. 5 ESI-MS analysis after 10 min irradiation ($\lambda_{cut\text{-}off} \geq 295$ nm) at pH 7.0 for the following conditions: (black) experiment with 30 μM iohexol, 3.0 mg L^{-1} humic acids, and 5.5 mg L^{-1} ClO^-; (blue) control A, lacking humic acids; (red) control B, lacking ClO^-; and (green) control C, lacking iohexol. Each spectrum represents the difference between the 10 min and corresponding 0 min time points. Labeled *m/z* values are color-coded to match the spectrum in which they appear with the highest intensity.

As iodide, registered at *m/z* 127 in the ESI-MS of Fig. 4 and 5, is released from iohexol, it is further oxidized, as recognised in previous studies.[8,15,49] For example, it can form molecular hypoiodite (IO^-), iodine (I_2), iodate (IO_3^-), and triiodide (I_3^-), which are respectively observed at *m/z* 143, 254 (for I_2^- anion), 175, and 381 in the ESI-MS of Fig. 4 and 5. The formation of these species is key due to their involvement the reactions described in the previous section.[14,38,54–58] Although IO_3^- can form *via* reaction R13, the detection of a peak at *m/z* 175 under conditions excluding iohexol (control C) suggests the formation of an alternative, non-iodine-containing species. In the absence of iohexol, the degradation of humic acids produces smaller organic compounds, resulting in a distinct shoulder peak in the mass spectrum (Fig. 5), offset by 0.31 amu from the iodate peak. This observation clearly indicates that the *m/z* 175 signal observed under the conditions of control C in Fig. 5 originates from an organic species rather than from iodate.

Iodine atoms ($I^\bullet$) can recombine to form I_2 (*m/z* 254) *via* reaction R17 with a rate constant $k_{R17} \approx 10^{10}$ M^{-1} s^{-1}.[59]

$$I^\bullet + I^\bullet \rightarrow I_2 \quad (R17)$$

This molecular iodine can subsequently react with water to produce HOI and I^- (reaction R18) $k_{R18} = 3.0$ s^{-1},[60] and with I^- to form I_3^- (reaction R19), with rate constants for the forward and backward reactions $k_{R19} = 6.2 \times 10^9$ M^{-1} s^{-1} and $k_{-R19} = 8.5 \times 10^6$ M^{-1} s^{-1}, respectively.[60]

$$I_2 + H_2O \rightarrow HOI + I^- + H^+ \quad (R18)$$

$$I_2 + I^- \rightleftarrows I_3^- \quad \text{(R19)}$$

Concurrently, hypochlorite degrades *via* reactions R15, and R16 to form chlorate (ClO_3^-), a unique species observed at *m/z* 83 and 85 with the expected isotopic signature ratio for 83 : 85 of 100.0% : 32.5%.

Chlorine substitution for iodine on the iohexol molecule, as described in Scheme 3 (reactions R20), yields a product at *m/z* 728 corresponding to the anion $C_{19}H_{25}I_2ClN_3O_9^-$ (iohexol − I + Cl) formed by a photodeiodination-coupled radical attack pathway. The dominant peak at *m/z* 728 is confirmed by its isotopic distribution at *m/z* 728 : 729 : 730 : 731 which is within experimental error of the theoretical intensity ratio values of 100.0% : 22.0% : 36.3% : 7.6% (Fig. S3). The isotopic pattern of two additional chlorine-substituted products discussed later is presented also in Fig. S3.

While the above chlorinated species are present under experimental conditions (Fig. 4), hydroxylated products are more prominent in the absence of hypochlorite, indicating competitive substitution by chlorine atoms. As shown by the red spectrum in Fig. 5, peaks at *m/z* 710, 600, and 490 are enhanced under chlorine-free conditions. These three peaks correspond to the stepwise substitution of iodine atoms on the iohexol ring with hydroxyl groups, as illustrated in Scheme 3 through reactions R21–R22. Specifically, these reactions yield *m/z* 710 (iohexol − I + OH), *m/z* 600 (iohexol − 2I + 2OH), and *m/z* 490 (iohexol − 3I + 3OH). These species are formed sequentially, with each transformation involving the loss of one iodine atom and the addition of one hydroxyl group.

The previous hydroxylated species should be capable of undergoing further transformation through intramolecular elimination,[61] facilitated by the conformational freedom of the side chains in iohexol. This process, in agreement with the literature,[41,62] leads to the formation of carbonyl-containing products shown in Scheme 3 that are observed in Fig. 5 at *m/z* 692 (iohexol − I − H), reaction R24 in Scheme 3, 582 (iohexol − I − HI + OH, reaction R25), and *m/z* 472 (iohexol − 2I − HI + 2OH, reaction R26).

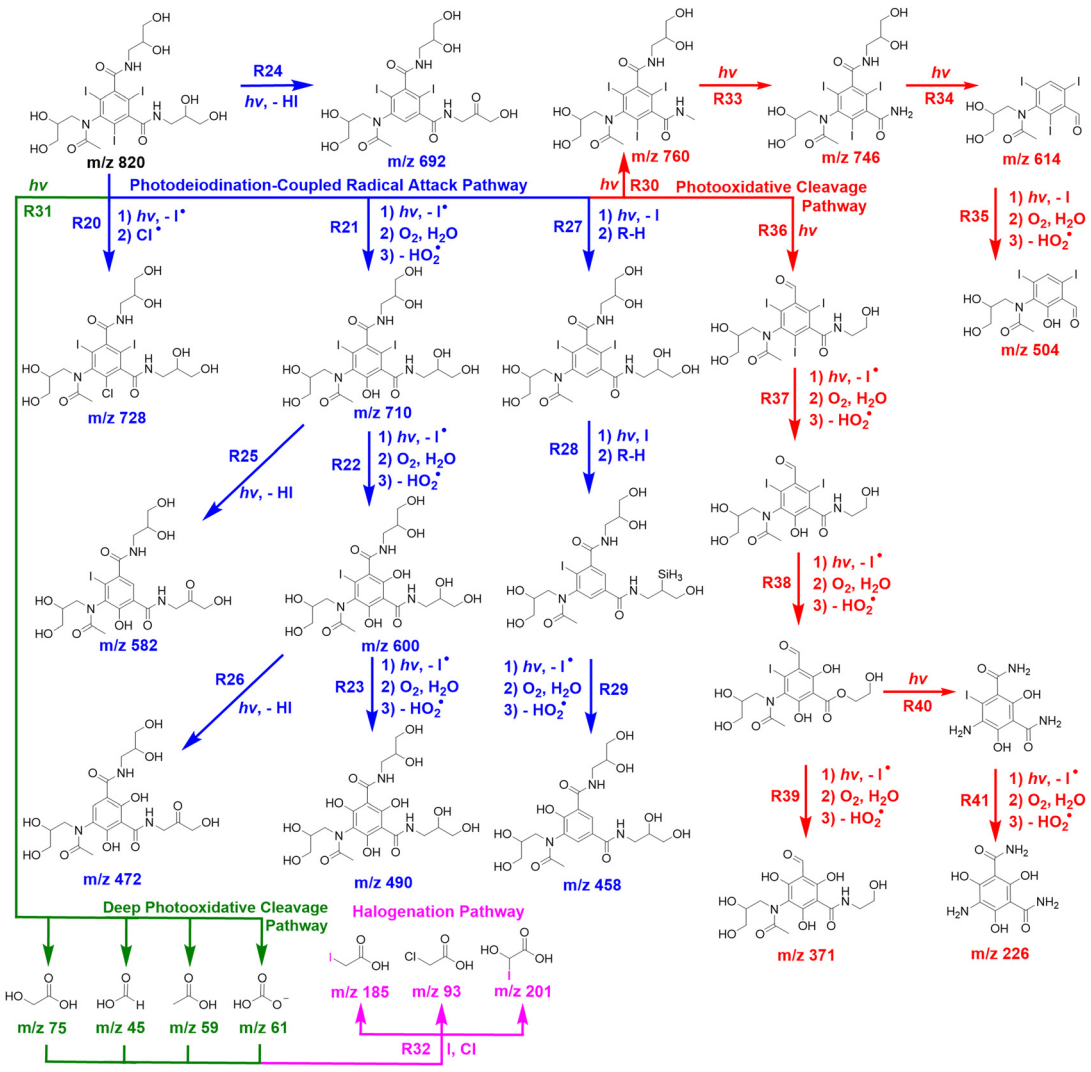

Scheme 3 Proposed irradiation/chlorination mechanism of iohexol transformation with color-coded observed *m/z* values corresponding to (blue) photodeiodination-coupled radical attack, (red) photooxidative cleavage, (green) deep photooxidative cleavage, and (pink) halogenation pathways.

Additionally, if the phenoxyl radical formed from the loss of iodine on the iohexol ring in Scheme 2 abstracts a hydrogen atom from a donor (symbolized as R–H in Scheme 3), the resulting product fills the vacant ring position and is 126 amu lighter than the parent compound. Given the abundance of iohexol in the experiment, this hydrogen is likely abstracted from another iohexol molecule during the initial kinetics, particularly from the secondary amide group as the bond dissociation energy follows the order N–H < C–H, O–H.[61] This pathway results in the formation of the product registered in Fig. 5 at *m*/*z* 458 (iohexol − 3I + OH), as described in reactions R27–R28–R29 of Scheme 3.

The photooxidative cleavage of iohexol can also lead to the loss of its branched side chains (reaction R30 in Scheme 3), producing larger fragments with *m*/*z* values of 760, 746, 614, 504, 371, 226, 194, and 162. Further multistep photooxidative cleavage represented by reaction R31 in Scheme 3 yields smaller products such as glycolic acid (*m*/*z* 75), bicarbonate (*m*/*z* 61) formed from CO_2(aq) made available from decarboxylation reactions, acetic acid (*m*/*z* 59), and formic acid (*m*/*z* 45). These smaller compounds can participate in the formation of hazardous disinfection byproducts (DBPs) through halogenation in the presence of chlorine and iodine and collectively represented by reaction R32 (Scheme 3). Alternatively, free halogens can react with humic substances to similarly form DBPs.[8,15]

Identified DBPs in present ESI-MS data (Fig. 4 and 5) *via* reaction R31 include chloroacetic acid (CAA, *m*/*z* 93), IAA (*m*/*z* 185), and hydroxyiodoacetic acid (*m*/*z* 201). CAA was confirmed by its isotopic peak at *m*/*z* 95 with a 93 : 95 ratio of 100.0% : 32.0% (Fig. S3). In the experiment corresponding to Fig. 4, the concentration of IAA was quantified as 0.16 μM by standard addition.

Photooxidative reactions R33 through R41 are provided to explain the observation of anions at *m*/*z* 746, 614, 504, 371, and 276 during ESI-MS analyses.

Implications for the toxicity of iodinated DBPs

The toxicity of DBPs is higher for iodinated compounds, as it is primarily influenced by the leaving group strength: $I^- > Br^- > Cl^- > F^-$.[63] These DBPs act as alkylating agents, readily reacting with deoxyribonucleic acid (DNA) nucleophiles and initiating tumorigenesis.[63] I-DBPs are known to be more cytotoxic and genotoxic than their chlorinated and brominated analogues.[6] Among these, iodinated haloacetic acids (I-HAAs), particularly the IAA identified in this work, exhibit higher toxicity than iodinated trihalomethanes (I-THMs), even at low (μM) concentrations.[8] Toxicity decreases with increasing halogenation, *e.g.*, IAA > diiodoacetic acid (DIAA),[4] while heterohalogenated HAAs like bromochoroacetic acid (BCAA) and bromoiodoacetic acid (BIAA) show similar toxicity profiles to each other.[4] Toxicity data for the lethal concentration (LC_{50}) for chlorinated and iodinated DBPs of interest are summarized in Fig. S4. For example, Fig. S4 shows that IAA exhibits the highest toxicity among the studied disinfection DBPs, with a lethal concentration for 50% of the population (LC_{50}) of 2.95×10^{-6} M and a significant toxicity threshold as low as 5.00×10^{-7} M.[6] Iodinated phenols (2-iodophenol, 4-iodophenol, and 2,6-diiodophenol) follow in relative toxicity with LC_{50} values of 6.01×10^{-4} M, 2.16×10^{-4} M, and 3.32×10^{-5} M, respectively.[64,65] The heterohalogenated chloroiodoacetic acid (CIAA) also falls within this range ($LC_{50} = 3.04 \times 10^{-4}$ M).[65] In contrast, chlorinated DBPs such as dichloroacetic acid (DCAA), trichloroacetic acid (TCAA), and chloroacetic acid (CAA) show the lowest toxicity, with LC_{50} values of 7.30×10^{-3} M, 2.40×10^{-3} M, and 8.10×10^{-3} M, respectively.[4,66] Genotoxicity comparisons further highlight IAA's potency, with a genotoxic threshold of 8.70×10^{-6} M compared to 4.10×10^{-4} M for CAA.[4,6]

Based on the experimentally determined [IAA] = 0.16 μM and applying a 200× dilution factor (accounting for a 200× higher [iohexol] in the experiment) we estimate that an environmental [IAA] of 0.8 nM could be generated during wastewater treatment. Considering a 150% increase in iodinated contrast media (ICM) usage from 2021 to 2024,[16] and assuming continued growth, [IAA] could reach 1.5 nM by *ca.* 2031. However, additional contributions from other hospitals, that were not considered in this estimation, may further elevate this concentration. Although current levels are below acute toxicity or genotoxic thresholds, chronic exposure to IAA may still pose health risks, including dental erosion, ulcers, headaches, fever, throat irritation, and skin conditions.[13,67]

The presence of I-DBPs, such as IAA, in receiving water bodies (even at nanomolar concentrations) raises significant ecological concerns due to their high cytotoxicity and genotoxicity.[9,68] Aquatic organisms, including fish, invertebrates, and microbial communities, may be particularly vulnerable to chronic exposure, which can lead to DNA damage, reproductive effects, developmental abnormalities, and shifts in ecological balance.[69] These risks are amplified in environments with elevated natural organic matter, where I-DBPs may persist and interact with other pollutants, potentially increasing their toxicity and environmental footprint.[9] Although current environmental concentrations of IAA in wastewater effluents and receiving freshwater systems remain below acute toxicity thresholds, its persistence and biological potency warrant expanded monitoring of I-DBPs and their consideration within regulatory frameworks for emerging contaminants (potentially including drinking water standards and surface water quality guidelines).[13,70] Including iodinated species in water quality assessments is essential to better evaluate and mitigate their long-term impact on ecosystem health.[70]

Finally, while low-molecular-weight DBPs, such as IAA, are recognized contributors to cytotoxicity in disinfected waters, recent research highlights the need to examine the largely uncharacterized high-molecular-weight DBP fraction.[71] Known one- and two-carbon DBPs may account for only a portion of observed toxicity, suggesting that larger, more

complex DBPs may be key drivers of health risks. Expanding analytical efforts to include these high-molecular-weight compounds is therefore essential for a more comprehensive understanding of DBP-related toxicity in freshwater and drinking water systems.[71]

Conclusions

Through the combined processes of irradiation and chlorination of the ICM iohexol, this study advances the mechanistic understanding of iodine ejection, the role of matrix components, and the formation of carcinogenic iodinated disinfection byproducts (I-DBPs). The initial deiodination of iohexol can proceed *via* multiple pathways, but direct photolysis appears to dominate under sunlight conditions, over hydroxyl radical and chlorine driven attack to the ring. After photo-ejection of iodine, hypochlorite appears to be particularly prominent, as evidenced by the formation of hydroxylated products. Even in the absence of added hypochlorite, such hydroxylated products are abundant, suggesting that dissolved O_2(aq) plays a key role in the radical-mediated pathway.

In addition to the generation of less toxic iohexol-derived fragments, the process also yields smaller, more hazardous haloacetic acids, such as IAA, which was confirmed and quantified in this study. The detection of IAA, even at low micromolar concentrations, raises significant concerns due to its known cytotoxic and genotoxic properties. These findings underscore the potential health risks associated with the growing discharge of treated hospital effluents into municipal wastewater systems.

While this study focuses on wastewater treatment, it is important to consider that iohexol or iodine species released from iohexol (and other ICM), such as I^- and HOI, may persist in surface waters and enter drinking water sources. During drinking water disinfection, particularly with chlorine or chloramine, these iodine precursors can react with NOM to form I-DBPs such as IAA and I-THMs, which are known for their elevated toxicity.[9,12,68] Studies have shown that the presence of ICM in source waters can significantly increase the formation potential of I-DBPs during drinking water treatment.[10] Given the higher genotoxicity and cytotoxicity of I-DBPs compared to their chlorinated and brominated analogues, their occurrence in drinking water systems poses a greater public health concern.[9] Therefore, monitoring iodine species and evaluating their transformation potential during drinking water treatment is critical to ensure the safety of potable water supplies.

Considering the persistence and potency of I-DBPs, particularly in environments rich in natural organic matter, further investigation into their formation pathways, environmental fate, and toxicological impacts is warranted. Quantitative assessments of I-DBPs in real-world hospital discharge scenarios are essential to evaluate their contribution to the overall DBP burden and to inform regulatory strategies aimed at minimizing public health risks.

Author contributions

Conceptualization, methodology, investigation, writing-reviewing and editing, formal analysis, data curation, writing-original draft preparation, and visualization: R. P. W. and M. I. G.; and resources, supervision, funding acquisition, and project administration: M. I. G. All authors have read and agreed to the final version of the manuscript.

Conflicts of interest

The authors declare no competing financial interest. The funders had no role in the design of the study, or interpretation of data; in the writing of the manuscript, or in the decision to publish this material.

Data availability

Supplementary information: Additional discussion, Scheme S1, Fig. S1–S4, and Table S1. See DOI: **https://doi.org/10.1039/D5EW00709G**.

All data supporting this article is provided in the document and in part in the SI.

Acknowledgements

Support from the U.S. National Science Foundation (NSF) under award number 2403875 is gratefully acknowledged. Additional support was provided through a University of Kentucky Research Traineeship Fellowship to R. P. W., funded under NSF award number 1922694.

References

1 C. H. Jeong, C. Postigo, S. D. Richardson, J. E. Simmons, S. Y. Kimura, B. J. Mariñas, D. Barcelo, P. Liang, E. D. Wagner and M. J. Plewa, Occurrence and comparative toxicity of haloacetaldehyde disinfection byproducts in drinking water, *Environ. Sci. Technol.*, 2015, **49**, 13749–13759, DOI: **10.1021/es506358x**, (accessed 2024-02-21).

2 M. G. Muellner, E. D. Wagner, K. McCalla, S. D. Richardson, Y.-T. Woo and M. J. Plewa, Haloacetonitriles vs. regulated haloacetic acids: are nitrogen-containing DBPs more toxic?, *Environ. Sci. Technol.*, 2007, **41**, 645–651.

3 M. J. Plewa, M. G. Muellner, S. D. Richardson, F. Fasano, K. M. Buettner, Y.-T. Woo, A. B. McKague and E. D. Wagner, Occurrence, synthesis, and mammalian cell cytotoxicity and genotoxicity of haloacetamides: an emerging class of nitrogenous drinking water disinfection byproducts, *Environ. Sci. Technol.*, 2008, **42**, 955–961.

4 M. J. Plewa, J. E. Simmons, S. D. Richardson and E. D. Wagner, Mammalian cell cytotoxicity and genotoxicity of the haloacetic acids, a major class of drinking water disinfection by-products, *Environ. Mol. Mutagen.*, 2010, **51**, 871–878.

5 M. J. Plewa, E. D. Wagner, P. Jazwierska, S. D. Richardson, P. H. Chen and A. B. McKague, Halonitromethane drinking water disinfection byproducts: chemical characterization

and mammalian cell cytotoxicity and genotoxicity, *Environ. Sci. Technol.*, 2004, **38**, 62–68.

6 S. D. Richardson, F. Fasano, J. J. Ellington, F. G. Crumley, K. M. Buettner, J. J. Evans, B. C. Blount, L. K. Silva, T. J. Waite and G. W. Luther, Occurrence and mammalian cell toxicity of iodinated disinfection byproducts in drinking water, *Environ. Sci. Technol.*, 2008, **42**, 8330–8338.

7 S. D. Richardson, M. J. Plewa, E. D. Wagner, R. Schoeny and D. M. DeMarini, Occurrence, genotoxicity, and carcinogenicity of regulated and emerging disinfection by-products in drinking water: a review and roadmap for research, *Mutat. Res., Rev. Mutat. Res.*, 2007, **636**, 178–242.

8 H. Dong, Z. Qiang and S. D. Richardson, Formation of iodinated disinfection byproducts (I-DBPs) in drinking water: emerging concerns and current issues, *Acc. Chem. Res.*, 2019, **52**, 896–905, DOI: **10.1021/acs.accounts.8b00641**, (acccessed 2023-02-28T15:27:42).

9 C. Postigo and B. Zonja, Iodinated disinfection byproducts: Formation and concerns, *Curr. Opin. Environ. Sci. Health*, 2019, **7**, 19–25, DOI: **10.1016/j.coesh.2018.08.006**.

10 S. D. Richardson and C. Postigo, Drinking Water Disinfection By-products, in *Emerging Organic Contaminants and Human Health*, ed. D. Barceló, Springer Berlin Heidelberg, 2012, pp. 93–137.

11 Food and Drug Administration, *OMNIPAQUE™ (iohexol) Injection*, ed. U.S. Departmentx of Agriculture, General Electric Company, 2017.

12 H. M. Dekker, G. J. Stroomberg and M. Prokop, Tackling the increasing contamination of the water supply by iodinated contrast media, *Insights Imaging*, 2022, **13**, 1–9.

13 Z. Zhu, A. Gross, P. B. Brown and G. Luo, Disinfection By-Products in Aquaculture: Sources, Impacts, Removal and Future Research, *Rev. Aquacult.*, 2025, **17**(3), e70035, DOI: **10.1111/raq.70035**.

14 Y. Bichsel and U. Von Gunten, Oxidation of iodide and hypoiodous acid in the disinfection of natural waters, *Environ. Sci. Technol.*, 1999, **33**, 4040–4045.

15 S. E. Duirk, C. Lindell, C. C. Cornelison, J. Kormos, T. A. Ternes, M. Attene-Ramos, J. Osiol, E. D. Wagner, M. J. Plewa and S. D. Richardson, Formation of toxic iodinated disinfection by-products from compounds used in medical imaging, *Environ. Sci. Technol.*, 2011, **45**, 6845–6854, DOI: **10.1021/es200983f**, (accessed 2023-03-06).

16 K. Ruf, *Iohexol/iodinated contrast media*, ed. R. Patton, 2024.

17 A. Sengar and A. Vijayanandan, Comprehensive review on iodinated X-ray contrast media: complete fate, occurrence, and formation of disinfection byproducts, *Sci. Total Environ.*, 2021, **769**, 1–23.

18 T. A. Ternes and R. Hirsch, Occurrence and behavior of X-ray contrast media in sewage facilities and the aquatic environment, *Environ. Sci. Technol.*, 2000, **34**, 2741–2748.

19 D. Weissbrodt, L. Kovalova, C. Ort, V. Pazhepurackel, R. Moser, J. Hollender, H. Siegrist and C. S. McArdell, Mass flows of X-ray contrast media and cytostatics in hospital wastewater, *Environ. Sci. Technol.*, 2009, **43**, 4810–4817.

20 Environmental Protection Agency, *Wastewater Technology Fact Sheet*, 2002, pp. 1–10.

21 K. L. Nelson, A. B. Boehm, R. J. Davies-Colley, M. C. Dodd, T. Kohn, K. G. Linden, Y. Liu, P. A. Maraccini, K. Mcneill and W. A. Mitch, *et al.*, Sunlight-mediated inactivation of health-relevant microorganisms in water: a review of mechanisms and modeling approaches, *Environ. Sci.: Processes Impacts*, 2018, **20**, 1089–1122, DOI: **10.1039/c8em00047f**, (accessed 2024-12-11).

22 R. C. Averett, J. Leenheer, D. M. McKnight and K. Thorn, *Humic substances in the Suwannee River, Georgia: Interactions, properties, and proposed structures*, US Government Printing Office, 1994.

23 Lexington-Fayette Urban County Government, *Sanitary sewer system and treatment plants*, 2025, **https://www.lexingtonky.gov/government/departments-programs/environmental-quality-public-works/water-quality/sanitary-sewer-system-treatment-plants** (accessed).

24 Environmental Protection Agency, *Quality Criteria for Water*, EPA, 1986, pp. 1–395.

25 Y. Gu, Z. Song, Z. Dong, F. Sun, C. Jiang and J. Qi, Efficient degradation and deiodination of iopamidol by UV/sulfite process: Assessment of typical process parameters and transformation paths, *Environ. Int.*, 2022, **167**, 1–10.

26 D. R. Lide, *CRC handbook of chemistry and physics: a ready-reference book of chemical and physical data*, CRC Press, 1995.

27 A. Imai, T. Fukushima, K. Matsushige, Y.-H. Kim and K. Choi, Characterization of dissolved organic matter in effluents from wastewater treatment plants, *Water Res.*, 2002, **36**, 859–870.

28 W. Kördel, M. Dassenakis, J. Lintelmann and S. Padberg, The importance of natural organic material for environmental processes in waters and soils (Technical Report), *Pure Appl. Chem.*, 1997, **69**, 1571–1600.

29 A. J. Eugene and M. I. Guzman, Reactivity of Ketyl and Acetyl Radicals from Direct Solar Actinic Photolysis of Aqueous Pyruvic Acid, *J. Phys. Chem. A*, 2017, **121**(15), 2924–2935, DOI: **10.1021/acs.jpca.6b11916**.

30 A. J. Eugene and M. I. Guzman, Production of singlet oxygen ($^1O_2$) during the photochemistry of aqueous pyruvic acid: The effects of ph and photon flux under steady-state O_2(aq) concentration, *Environ. Sci. Technol.*, 2019, **53**, 12425–12432.

31 A. J. Eugene and M. I. Guzman, The effects of reactant concentration and air flow rate in the consumption of dissolved O_2 during the photochemistry of aqueous pyruvic acid, *Molecules*, 2019, **24**, 1–11.

32 A. J. Eugene, S.-S. Xia and M. I. Guzman, Aqueous Photochemistry of Glyoxylic Acid, *J. Phys. Chem. A*, 2016, **120**(21), 3817–3826, DOI: **10.1021/acs.jpca.6b00225**.

33 S.-S. Xia, A. J. Eugene and M. I. Guzman, Cross Photoreaction of Glyoxylic and Pyruvic Acids in Model Aqueous Aerosol, *J. Phys. Chem. A*, 2018, **122**(31), 6457–6466, DOI: **10.1021/acs.jpca.8b05724**.

34 H. Görner and H. J. Kuhn, Photodecarboxylation of phenylglyoxylic acid: Influence of para-substituents on the triplet state properties, *J. Chem. Soc., Perkin Trans. 2*, 1999, **12**, 2671–2680.

35 D. J. Price, *Site visit and tour of the Town Branch Laboratory and Wastewater Treatment Plant of the Lexington Division of Water Quality*, ed. R. P. Witt and M. I. Guzman, 2024.
36 E. Borowska, E. Felis and S. Żabczyński, Degradation of iodinated contrast media in aquatic environment by means of UV, UV/TiO 2 process, and by activated sludge, *Water, Air, Soil Pollut.*, 2015, **226**, 1–12.
37 S. S. Kabirhashemi and H. Eskandari, Deiodination of iohexol employing magnetic α-Ni (OH) 2/Ni nanoflakes for flow injection sensing of iohexol, *Sens. Actuators, B*, 2021, **348**, 130731.
38 S. V. Kireev and S. L. Shnyrev, Study of molecular iodine, iodate ions, iodide ions, and triiodide ions solutions absorption in the UV and visible light spectral bands, *Laser Phys.*, 2015, **25**, 1–11.
39 C. Fang, X. Luan, F. Ao, X. Wang, S. Ding, Z. Du, S. Liu, R. Jia and W. Chu, Decomposition of Total Organic Halogen Formed during Chlorination: The Iceberg of Halogenated Disinfection Byproducts Was Previously Underestimated, *Environ. Sci. Technol.*, 2023, **57**(3), 1433–1442, DOI: **10.1021/acs.est.2c03596**.
40 A. Levy, D. Meyerstein and M. Ottolenghi, Photochemically induced isotopic exchange between iodobenzene and molecular iodine, *J. Phys. Chem.*, 1971, **75**, 3350–3354.
41 J. Jeong, J. Jung, W. J. Cooper and W. Song, Degradation mechanisms and kinetic studies for the treatment of X-ray contrast media compounds by advanced oxidation/reduction processes, *Water Res.*, 2010, **44**, 4391–4398.
42 R. Grossman, *The Art of Writing Reasonable Organic Reaction Mechanisms*, Springer, 2003.
43 P. Klan and J. Wirz, *Photochemistry of Organic Compounds from Concepts to Practice*, John Wiley & Sons, 2009.
44 P. Neta and J. Grodkowski, Rate Constants for Reactions of Phenoxyl Radicals in Solution, *J. Phys. Chem. Ref. Data*, 2005, **34**(1), 109–199, DOI: **10.1063/1.1797812**, (accessed 2025-06-25).
45 Y. Lei, S. Cheng, N. Luo, X. Yang and T. An, Rate Constants and Mechanisms of the Reactions of $Cl^{\bullet}$ and $Cl_2^{\bullet-}$ with Trace Organic Contaminants, *Environ. Sci. Technol.*, 2019, **53**(19), 11170–11182, DOI: **10.1021/acs.est.9b02462**.
46 L. H. Nowell and J. Hoigné, Photolysis of aqueous chlorine at sunlight and ultraviolet wavelengths—I. Degradation rates, *Water Res.*, 1992, **26**(5), 593–598, DOI: **10.1016/0043-1354(92)90232-S**.
47 D. M. Bulman, S. P. Mezyk and C. K. Remucal, The impact of pH and irradiation wavelength on the production of reactive oxidants during chlorine photolysis, *Environ. Sci. Technol.*, 2019, **53**, 4450–4459.
48 F. M. Wendel, C. Lütke Eversloh, E. J. Machek, S. E. Duirk, M. J. Plewa, S. D. Richardson and T. A. Ternes, Transformation of iopamidol during chlorination, *Environ. Sci. Technol.*, 2014, **48**, 12689–12697, DOI: **10.1021/es503609s**, (accessed 2023-03-06).
49 F. M. Wendel, T. A. Ternes, S. D. Richardson, S. E. Duirk, J. A. Pals, E. D. Wagner and M. J. Plewa, Comparative toxicity of high-molecular weight iopamidol disinfection byproducts, *Environ. Sci. Technol. Lett.*, 2016, **3**, 81–84.
50 H.-H. Jiang, L.-M. Cai, H.-H. Wen, G.-C. Hu, L.-G. Chen and J. Luo, An integrated approach to quantifying ecological and human health risks from different sources of soil heavy metals, *Sci. Total Environ.*, 2020, **701**, 1–11.
51 F.-X. Tian, B. Xu, Y.-L. Lin, C.-Y. Hu, T.-Y. Zhang, S.-J. Xia, W.-H. Chu and N.-Y. Gao, Chlor(am)ination of iopamidol: kinetics, pathways and disinfection by-products formation, *Chemosphere*, 2017, **184**, 489–497.
52 Z. Wang, Y.-L. Lin, B. Xu, S.-J. Xia, T.-Y. Zhang and N.-Y. Gao, Degradation of iohexol by UV/chlorine process and formation of iodinated trihalomethanes during post-chlorination, *Chem. Eng. J.*, 2016, **283**, 1090–1096.
53 M. Lister, Decomposition of sodium hypochlorite: the uncatalyzed reaction, *Can. J. Chem.*, 1956, **34**, 465–478.
54 A. Allen, The yields of free H and OH in the irradiation of water, *Radiat. Res.*, 1954, **1**, 85–96.
55 Y. Guo, K. Li, S. Perrier, T. An, D. J. Donaldson and C. George, Spontaneous iodide activation at the air–water interface of aqueous droplets, *Environ. Sci. Technol.*, 2023, **57**, 15580–15587.
56 J. K. Lee, K. L. Walker, H. S. Han, J. Kang, F. B. Prinz, R. M. Waymouth, H. G. Nam and R. N. Zare, Spontaneous generation of hydrogen peroxide from aqueous microdroplets, *Proc. Natl. Acad. Sci. U. S. A.*, 2019, **116**, 19294–19298.
57 M. A. Mehrgardi, M. Mofidfar and R. N. Zare, Sprayed water microdroplets are able to generate hydrogen peroxide spontaneously, *J. Am. Chem. Soc.*, 2022, **144**, 7606–7609.
58 J. Li, J. Jiang, S. Y. Pang, Y. Cao, Y. Zhou and C. Guan, Oxidation of iodide and hypoiodous acid by non-chlorinated water treatment oxidants and formation of iodinated organic compounds: A review, *Chem. Eng. J.*, 2020, **386**, 1–10.
59 G. Foldiak and R. H. Schuler, Rate constants for the scavenging of radicals by iodine, *J. Phys. Chem.*, 1978, **82**, 2756–2757.
60 R. C. Troy, M. D. Kelley, J. C. Nagy and D. W. Margerum, Non-metal redox kinetics: Iodine monobromide reaction with iodide ion and the hydrolysis of IBr, *Inorg. Chem.*, 1991, **30**, 4838–4845.
61 D. Klein, *Organic Chemistry*, John Wiley and Sons Inc., 2015.
62 S. Giannakis, M. Jovic, N. Gasilova, M. P. Gelabert, S. Schindelholz, J.-M. Furbringer, H. Girault and C. Pulgarin, Iohexol degradation in wastewater and urine by UV-based Advanced Oxidation Processes (AOPs): Process modeling and by-products identification, *J. Environ. Manage.*, 2017, **195**, 174–185.
63 M. Loudon, *Organic Chemistry*, Addison-Wesley Pub. Co., 1984.
64 H. K. Liberatore, M. J. Plewa, E. D. Wagner, J. M. VanBriesen, D. B. Burnett, L. H. Cizmas and S. D. Richardson, Identification and Comparative Mammalian Cell Cytotoxicity of New Iodo-Phenolic Disinfection

Byproducts in Chloraminated Oil and Gas Wastewaters, *Environ. Sci. Technol.*, 2017, **4**(11), 475–480, DOI: **10.1021/acs.estlett.7b00468**.

65 E. D. Wagner and M. J. Plewa, CHO cell cytotoxicity and genotoxicity analyses of disinfection by-products: An updated review, *J. Environ. Sci.*, 2017, **58**, 64–76, DOI: **10.1016/j.jes.2017.04.021**.

66 S. S. Lau, X. Wei, K. Bokenkamp, E. D. Wagner, M. J. Plewa and W. A. Mitch, Assessing Additivity of Cytotoxicity Associated with Disinfection Byproducts in Potable Reuse and Conventional Drinking Waters, *Environ. Sci. Technol.*, 2020, **54**(9), 5729–5736, DOI: **10.1021/acs.est.0c00958**.

67 Santa Cruz Biotechnology Inc., *Iodoacetic acid*, 2010, **https://datasheets.scbt.com/sc-215183.pdf** (accessed 2025-06-26).

68 H. MacKeown, U. von Gunten and J. Criquet, Iodide sources in the aquatic environment and its fate during oxidative water treatment – A critical review, *Water Res.*, 2022, **217**, 118417, DOI: **10.1016/j.watres.2022.118417**.

69 M. L. Hladik, L. E. Hubbard, D. W. Kolpin and M. J. Focazio, Dairy-Impacted Wastewater Is a Source of Iodinated Disinfection Byproducts in the Environment, *Environ. Sci. Technol. Lett.*, 2016, **3**(5), 190–193, DOI: **10.1021/acs.estlett.6b00109**.

70 R. El Sayess, *Total Organic Iodine Quantification and Occurrence in Drinking Water, and Toxicity Assessment of Iodinated Disinfection By-Products*, 2017, **https://scholarworks.umass.edu/entities/publication/03bcd6d6-296f-46d8-97ae-88952e15cb71** (accessed 2025-08-26).

71 W. A. Mitch, S. D. Richardson, X. Zhang and M. Gonsior, High-molecular-weight by-products of chlorine disinfection, *Nat. Water*, 2023, **1**(4), 336–347, DOI: **10.1038/s44221-023-00064-x**.